

Second harmonic generation from exfoliated hexagonal boron nitride flakes

Sejeong Kim^{1,†}, Johannes E. Fröch¹, Augustine Gardner¹, Chi Li¹, Igor Aharonovich¹, and Alexander S. Solntsev^{1,†}

¹School of Mathematical and Physical Sciences, University of Technology Sydney, Ultimo, New South Wales, 2007, Australia

[†]E-mail: Sejeong.Kim-1@uts.edu.au, Alexander.Solntsev@uts.edu.au

Abstract

We report second harmonic generation (SHG) from thick hexagonal boron nitride (hBN) flakes with approximately 108-109 layers. Surprisingly, the resulting signal is stronger when compared to previously reported few-layer experiments that showed the SHG efficiency decreasing with the increasing thickness. This confirms that thick hBN flakes can serve as a platform for nonlinear optics, which is useful because thick flakes are easy to exfoliate while retaining a large flake size. We also show spatial second harmonic maps revealing that SHG remains a useful tool for the characterization of the layer structure even in the case of a large number of layers.

Keywords: second harmonic generation, 2D material, hexagonal boron nitride, nonlinear optics

1. Introduction

Layered materials comprise an extremely promising class of materials for optics and photonics. The most widely studied layered materials are graphene [1], hexagonal boron nitride [2], and transition metal dichalcogenides (TMDCs) such as MoS₂, WS₂, MoSe₂, and WSe₂ [3]. TMDCs and hBN have a direct band gap and show bright photoluminescence [4, 5] and strong second harmonic generation [6].

Second harmonic generation is particularly important in this context because it allows quantifying quadratic nonlinear optical susceptibility ($\chi^{(2)}$) of these layered materials [7-9] for the purpose of potential integration with well-developed photonic platforms such as silicon on insulator [10], silicon nitride on insulator [11] or aluminum nitride on insulator [12]. These platforms have near zero $\chi^{(2)}$, and thus adding a thin layer of material with strong $\chi^{(2)}$ on top of a photonic structure [13, 14] may enable a range of $\chi^{(2)}$ -based applications such as nonlinear spectroscopy [15] and nonlinear signal processing [16, 17].

Furthermore, SHG can be used to study the layer structure of layered materials. Typically, $\chi^{(2)}$ would be strong for odd numbers of layers and near zero for even numbers of layers due to interference [18], although it also depends on the orientation between the layers [19, 20]. Thus nonlinear spectroscopy of layered materials has become a useful tool to determine the crystalline orientation, thickness uniformity, layer stacking and flake sizes [6].

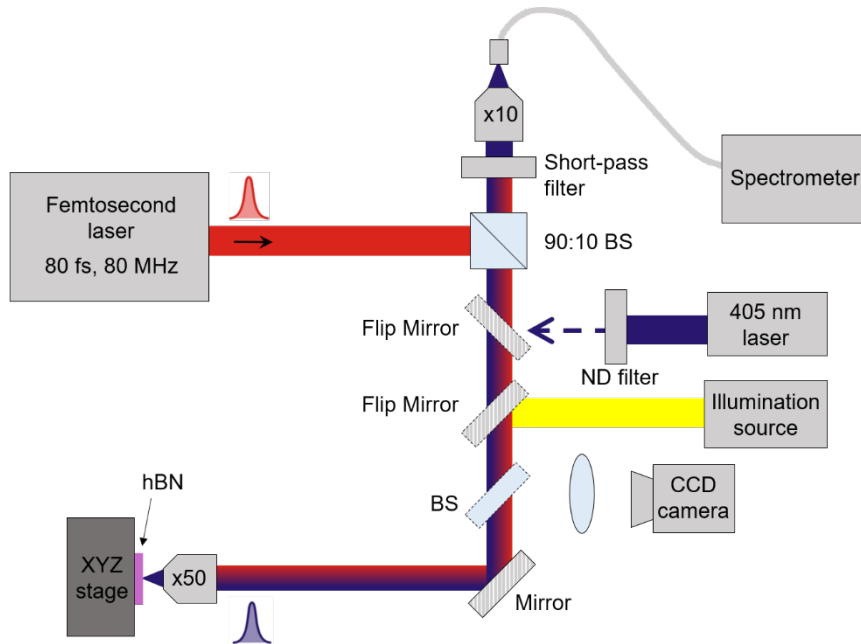


Figure 1. Home-built experimental setup for optical characterizations. A femtosecond laser is used to measure second harmonic response of hexagonal Boron Nitride (BS: beam splitter, ND filter: neutral density filter).

The case of SHG in hBN has also been studied [18, 19, 21, 22], but less intensively compared to TMDCs, likely due to lower $\chi^{(2)}$ [6]. However, one of the big advantages of hBN is its transparency in the entire visible range, potentially opening doors for visible nonlinear optical applications [23].

In this work, we confirm experimentally that, despite projections from earlier 1-to-5 layers experiments [18] indicating a decrease of SHG efficiency with increasing hBN thickness, strong SHG can be achieved in hBN with above 100 layers, enabling the use of thick mechanically exfoliated hBN lakes in nonlinear optics.

2. Methods

The optical measurement setup used for the characterization is shown in figure 1. A femtosecond pulsed laser with 80 MHz repetition rate is used as an excitation laser. The width of the pulse is measured to be 80 fs. The pump laser is focused through a 50 x objective lens with a numerical aperture of 0.55, and the same objective lens was used to collect the second harmonic signal from the hBN. The hBN sample is mounted on the piezo-stage, and the second-harmonic signal is measured by a spectrometer (QEpro, OceanOptics) to show spectra and 2D mapping.

To convert intensity values measured at the spectrometer to the power generated from the sample, the system is calibrated using the laser with the same wavelength as the second harmonic signal. 405

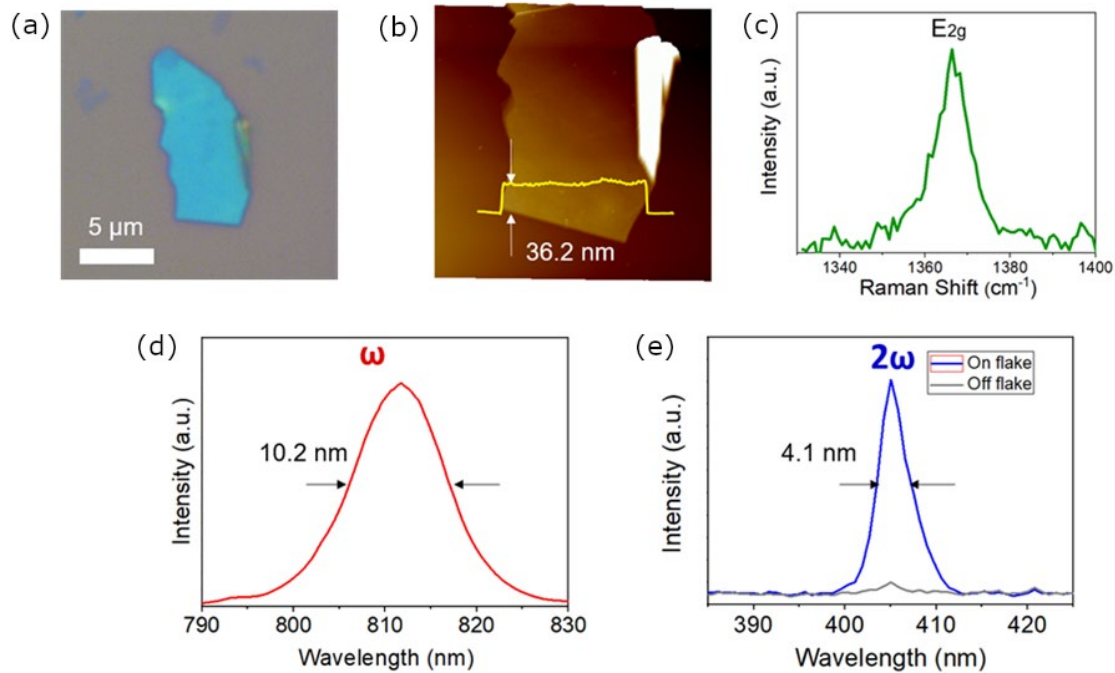


Figure 2. Second harmonic generation (SHG) from an hBN flake. (a) Optical image of the studied mechanically exfoliated hBN flake. (b) Atomic force microscopy (AFM) map of the flake showing the thickness of flake corresponding to 36.2 nm. (c) Raman spectrum of the hBN flake. (d) The pump laser wavelength at 810 nm with full-width half-maximum (FWHM) of 10.2 nm. (e) SHG from hBN flake (blue solid line) with FWHM of 4.1 nm. Grey line shows the negligible signal from the SiO₂ substrate.

nm laser shown in figure 1 is attenuated by the ND filter and directly measured by the spectrometer. The transmission of the objective lens at 405 nm is also measured for system calibration.

For sample preparation, the hBN bulk crystal was mechanically exfoliated on a SiO₂ substrate. The sample was heated in air at 500°C and subsequently annealed in vacuum at 850°C temperature for 30 minutes to clean the top surface. An optical microscope image of the transferred flake is shown in figure 2(a). The same hBN flake is analyzed using atomic force microscopy (AFM) and Raman spectroscopy. Figure 2(b) shows the thickness of the flake is 36.2 nm. Monolayer thickness of hBN is known to be 0.33 nm, therefore the flake shown in figure 1 has about 108-109 layers. Raman spectroscopy was used to identify hBN crystalline structure showing the characteristic hBN E_{2g} Raman mode at 1366 cm⁻¹ as shown in figure 2(c). The flake was further characterized by photoluminescence. Figure 2(d) shows the pump wavelength at 810 nm with a linewidth of 10.2 nm. The second harmonic signal is observed at 405 nm with a reduced linewidth of 4.1 nm as shown in figure 2(e). The line narrowing between the pump and the SHG signal is consistent with predictions based on conventional frequency doubling theory [<https://doi.org/10.1063/1.4915134>]. The gray line in figure 2(e) shows the negligible nonlinear response from the SiO₂ substrate.

3. Results and Discussion

3.1 SHG power versus pump power

Figure 3(a) shows power-dependent spectra of SHG from the hBN sample characterized in figure 2. The signal was collected from the center of the flake to avoid the edge effect. The excitation power in figure 3(a) was measured before the objective lens. To plot excitation power-dependent SHG power

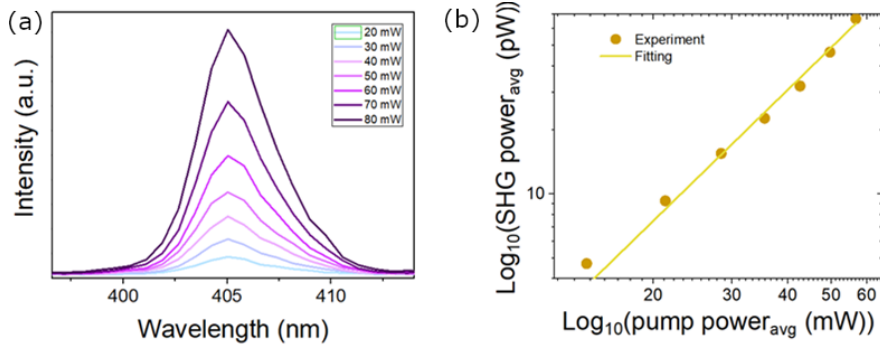


Figure 3. Power-dependent nonlinear response from hBN. (a) Excitation power-dependent SHG spectra. The pump power is measured before objective lens. Each spectrum in is integrated from 400 nm to 410 nm to get integrated intensity. The integrated intensity with arbitrary unit is converted into exact SHG power. (b) SHG power with respect to the excitation pump power on the sample.

to see the quadratic behavior, the values in figure 3(a) were carefully converted. First, the excitation power onto the hBN sample was derived from the power measured before objective multiplied by the transmission of the objective lens at 405 nm, which is in our case 0.709. Next, the integrated intensity from each spectrum with the arbitrary unit is converted into real power using the calibration explained in the Methods section. The Log-log plot (figure 3(b)) of the excitation power and SHG power showing a linear slope of 2.05 ± 0.126 .

3.2 The second-order susceptibility

The second order susceptibility of the studied hBN flake adjusted for its thickness is calculated using the following equation [8]:

$$|\chi_{th}^{(2)}| = \sqrt{\frac{P(2\omega) \times c \times \epsilon_0 \times RR \times A \times \Delta\tau \times \lambda^2 \times (1+n)^6}{64\sqrt{2}\pi^2 \times P^2(\omega) \times S \times n^3}}$$

Where $P(2\omega)$ is the average power from the second harmonic signal, $P(\omega)$ is the average power of the excitation laser, c is the speed of light in vacuum and ϵ_0 is the vacuum electric permittivity (8.85×10^{-12} F/m). RR is the repetition rate of the excitation laser (80 MHz), A is the pump spot area (3.14×10^{-12} m²), $\Delta\tau$ is the pulse full width at half maximum, and $S = 0.94$ is a shape factor for Gaussian pulses. Finally, a refractive index of SiO₂ ($n = 1.5$) is used. Here, the pump spot area (A) is identified from the CCD camera. From the equation shown above, we obtain a value of 0.81×10^{-20} m²/V. If we assume that only one layer with a thickness $d = 0.33$ nm is responsible for the SHG while other layers interfere destructively as suggested in earlier works [6, 18], then we get a value of a single-layer quadratic nonlinear optical susceptibility $\chi^{(2)} = \chi_{th}^{(2)}/d = 2.5 \times 10^{-11}$ m/V, which is a slightly higher than previously reported value for a single layer despite the expectations that quadratic nonlinearity should decrease when the number of layers increase [18]. A likely explanation for this phenomenon is a difference in the quality of the utilised hBN flakes.

3.3 2D mapping of SHG

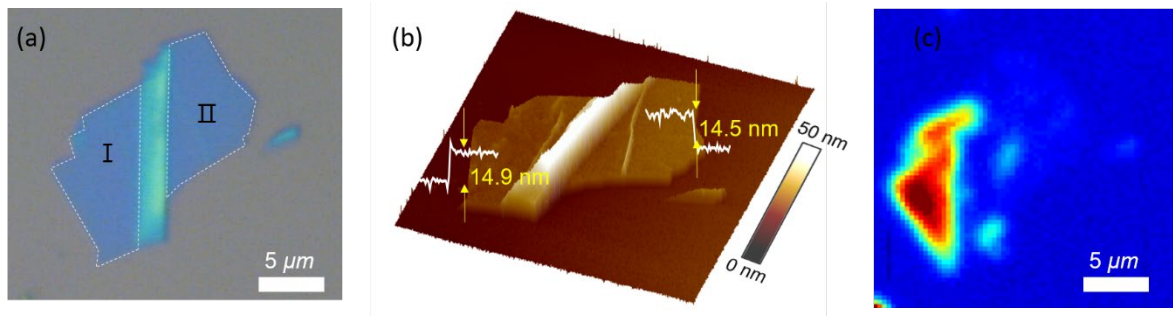


Figure 4. SHG spatial mapping. (a) Optical image of hBN flake with areas of different layer number labelled as I and II. (b) AFM map of the flake shown in (a). (c) Spatial SHG intensity mapping across hBN sample with excitation of 980 nm.

Due to the layered nature of hBN, the same flake may have a non-homogeneous thickness. Therefore, it is important to map the SHG from a given flake. An hBN flake shown in figure 4(a) is used to acquire a second harmonic spectroscopy map. The flake is analyzed using AFM and exhibits areas of different thickness, on the left (region I) and the right (region II) side with respect to the folded center line as shown in figure 4(b).

To construct an SHG 2D map at a particular wavelength, the sample was scanned with a piezo-stage while collecting a spectrum at each step. Subsequently, these spectra were post-processed to extract the intensity at the SHG value. Each pixel in the 2d map shows the intensity value at 405 nm in this case. This approach can avoid any possible noise that may affect SHG microscopy, which uses a sensitive CCD camera and a bandpass filter to construct the SHG 2D image. In figure 4(c), an excitation wavelength of 910 nm was used to pump the sample with an excitation laser measured before the objective lens corresponding to 40 mW. Collection time for each spectrum is 500 ms. Region I shows strong SHG signal while the signal from region II is negligible. This is because hBN layers are stacked in 2H order, where the sites for boron and nitride alternating when the layer increases. Therefore, the inversion symmetry is only broken for an odd number of layers. Based on the SHG mapping and the AFM analysis, region I has an odd number of stacked layers which is one layer thicker than region II.

4. Conclusion

We have demonstrated strong SHG from thick hBN flakes with above 100 layers. We have measured the normalized quadratic nonlinear optical susceptibility to be slightly higher than previously reported from single layers. We have also demonstrated with spatial mapping that SHG may be a good tool to characterize the layer structure of thick flakes. In the future, it will be interesting to test systems with intermediate thickness where the number of layers can be measured precisely, as well as to integrate hBN flakes with microstructures. Other potentially interesting research directions include experimental verification of theory for hBN SHG in deep-UV [21] and SHG in hBN nano-structures [22].

Acknowledgments

The authors acknowledge support from the Australian Research Council including DE180100070 and DP190101058.

References

- [1] Maier S A 2012 All eyes on flatland *Nature Physics* **8** 581
- [2] Wang J, Ma F and Sun M 2017 Graphene, hexagonal boron nitride, and their heterostructures: properties and applications *RSC Advances* **7** 16801-22
- [3] Mak K F and Shan J 2016 Photonics and optoelectronics of 2D semiconductor transition metal dichalcogenides *Nature Photonics* **10** 216-26
- [4] Novoselov K S, Mishchenko A, Carvalho A and Neto A H C 2016 2D materials and van der Waals heterostructures *Science* **353** aac9439
- [5] Kim S, Fröch J E, Christian J, Straw M, Bishop J, Totonjian D, Watanabe K, Taniguchi T, Toth M and Aharonovich I 2018 Photonic crystal cavities from hexagonal boron nitride *Nat Commun* **9** 2623
- [6] Autere A, Jussila H, Dai Y, Wang Y, Lipsanen H and Sun Z 2018 Nonlinear Optics with 2D Layered Materials *Adv Mater* **30** 1705963
- [7] Rosa H G, Ho Y W, Verzhbitskiy I, Rodrigues M, Taniguchi T, Watanabe K, Eda G, Pereira V M and Gomes J C V 2018 Characterization of the second- and third-harmonic optical susceptibilities of atomically thin tungsten diselenide *Scientific Reports* **8** 10035
- [8] Woodward R I, Murray R T, Phelan C F, de Oliveira R E P, Runcorn T H, Kelleher E J R, Li S, de Oliveira E C, Fechine G J M, Eda G and de Matos C J S 2017 Characterization of the second- and third-order nonlinear optical susceptibilities of monolayer MoS₂ using multiphoton microscopy *2d Mater* **4** 011006
- [9] Clark D J, Le C T, Senthilkumar V, Ullah F, Cho H Y, Sim Y, Seong M J, Chung K H, Kim Y S and Jang J I 2015 Near bandgap second-order nonlinear optical characteristics of MoS₂ monolayer transferred on transparent substrates *Applied Physics Letters* **107** 13
- [10] Inniss D and Rubenstein R 2016 *Silicon Photonics: Fueling the Next Information Revolution*: Morgan Kaufmann Publishers Inc.)
- [11] Muñoz P, Micó G, Bru L A, Pastor D, Pérez D, Doménech J D, Fernández J, Baños R, Gargallo B, Alemany R, Sánchez A M, Cirera J M, Mas R and Domínguez C 2017 Silicon Nitride Photonic Integration Platforms for Visible, Near-Infrared and Mid-Infrared Applications *Sensors (Basel, Switzerland)* **17** 2088
- [12] Lu T-J, Fanto M, Choi H, Thomas P, Steidle J, Mouradian S, Kong W, Zhu D, Moon H, Berggren K, Kim J, Soltani M, Preble S and Englund D 2018 Aluminum nitride integrated photonics platform for the ultraviolet to visible spectrum *Opt. Express* **26** 11147-60
- [13] Fryett T K, Seyler K L, Zheng J, Liu C-H, Xu X and Majumdar A 2017 Silicon photonic crystal cavity enhanced second-harmonic generation from monolayer WSe₂ *2d Mater* **4** 015031
- [14] Chen H, Corboliou V, Solntsev A S, Choi D-Y, Vincenti M A, de Ceglia D, de Angelis C, Lu Y and Neshev D N 2017 Enhanced second-harmonic generation from two-dimensional MoSe₂ on a silicon waveguide *Light: Science & Applications* **6** e17060
- [15] Solntsev A S, Kumar P, Pertsch T, Sukhorukov A A and Setzpfandt F 2018 LiNbO₃ waveguides for integrated SPDC spectroscopy *APL Photonics* **3** 021301
- [16] Schiek R, Solntsev A S and Neshev D N 2012 Temporal dynamics of all-optical switching in quadratic nonlinear directional couplers *Applied Physics Letters* **100** 111117
- [17] Srivastava Y K, Chaturvedi A, Manjappa M, Kumar A, Dayal G, Kloc C and Singh R 2017 MoS₂ for Ultrafast All-Optical Switching and Modulation of THz Fano Metaphotonic Devices *Adv Opt Mater* **5** 1700762
- [18] Li Y, Rao Y, Mak K F, You Y, Wang S, Dean C R and Heinz T F 2013 Probing Symmetry Properties of Few-Layer MoS₂ and h-BN by Optical Second-Harmonic Generation *Nano Letters* **13** 3329-33
- [19] Kim C-J, Brown L, Graham M W, Hovden R, Havener R W, McEuen P L, Muller D A and Park J 2013 Stacking Order Dependent Second Harmonic Generation and Topological Defects in h-BN Bilayers *Nano Letters* **13** 5660-5
- [20] Hsu W-T, Zhao Z-A, Li L-J, Chen C-H, Chiu M-H, Chang P-S, Chou Y-C and Chang W-H 2014 Second Harmonic Generation from Artificially Stacked Transition Metal Dichalcogenide Twisted Bilayers *ACS Nano* **8** 2951-8
- [21] Taghizadeh A and Pedersen T G 2018 Gauge invariance of excitonic linear and nonlinear optical response *Physical Review B* **97** 205432
- [22] Lucking M C, Beach K and Terrones H 2018 Large second harmonic generation in alloyed TMDs and boron nitride nanostructures *Scientific Reports* **8** 10118
- [23] Garmire E 2013 Nonlinear optics in daily life *Opt. Express* **21** 30532-44